

Serveur Académique Lausannois SERVAL [serval.unil.ch](http://serval.unil.ch)

## Author Manuscript

Faculty of Biology and Medicine Publication

This paper has been peer-reviewed but does not include the final publisher proof-corrections or journal pagination.

Published in final edited form as:

**Title:** Mutations in CEP78 Cause Cone-Rod Dystrophy and Hearing Loss Associated with Primary-Cilia Defects.

**Authors:** Nikopoulos K, Farinelli P, Giangreco B, Tsika C, Royer-Bertrand B, Mbefo MK, Bedoni N, Kjellström U, El Zaoui I, Di Gioia SA, Balzano S, Cisarova K, Messina A, Decembrini S, Plainis S, Blazaki SV, Khan MI, Micheal S, Boldt K, Ueffing M, Moulin AP, Cremers FP, Roepman R, Arsenijevic Y, Tsilimbaris MK, Andréasson S, Rivolta C

**Journal:** American journal of human genetics

**Year:** 2016 Sep 1

**Volume:** 99

**Issue:** 3

**Pages:** 770-6

**DOI:** 10.1016/j.ajhg.2016.07.009

In the absence of a copyright statement, users should assume that standard copyright protection applies, unless the article contains an explicit statement to the contrary. In case of doubt, contact the journal publisher to verify the copyright status of an article.

# REPORT

## Mutations in *CEP78* cause cone-rod dystrophy and hearing loss associated with primary cilia defects

Konstantinos Nikopoulos,<sup>1§</sup> Pietro Farinelli,<sup>1§</sup> Basilio Giangreco,<sup>2</sup> Chrysanthi Tsika,<sup>3</sup> Beryl Royer-Bertrand,<sup>1,4</sup> Martial K. Mbefo,<sup>5</sup> Nicola Bedoni,<sup>1</sup> Ulrika Kjellstrom,<sup>6</sup> Ikram El Zaoui,<sup>1</sup> Silvio Alessandro Di Gioia,<sup>1</sup> Sara Balzano,<sup>1</sup> Katarina Cisarova,<sup>1</sup> Andrea Messina,<sup>7</sup> Sarah Decembrini,<sup>5</sup> Sotiris Plainis,<sup>3</sup> Stella Mplazaki,<sup>3</sup> Muhammad Imran Khan,<sup>8</sup> Shazia Micheal,<sup>8</sup> Karsten Boldt,<sup>9</sup> Marius Ueffing,<sup>9</sup> Alexandre P. Moulin,<sup>10</sup> Frans P. Cremers,<sup>8,11</sup> Ronald Roepman,<sup>8</sup> Yvan Arsenijevic,<sup>5</sup> Miltiadis K. Tsilimbaris,<sup>3</sup> Sten Andréasson,<sup>6</sup> Carlo Rivolta<sup>1\*</sup>

<sup>§</sup> Equal contribution

\* Correspondence (carlo.rivolta@unil.ch)

<sup>1</sup>Department of Computational Biology, Unit of Medical Genetics, University of Lausanne, Lausanne, Switzerland

<sup>2</sup>Center for Psychiatric Neuroscience, Department of Psychiatry, Lausanne University Hospital, Lausanne, Switzerland

<sup>3</sup>Department of Ophthalmology, Medical School, University of Crete, Heraklion, Greece

<sup>4</sup>Center for Molecular Diseases, Lausanne University Hospital, Lausanne, Switzerland

<sup>5</sup>Unit of Gene Therapy and Stem Cell Biology, Jules Gonin Ophthalmic Hospital, Lausanne, Switzerland

<sup>6</sup>Lund University, Skane University Hospital, Department of Ophthalmology, Lund, Sweden

<sup>7</sup>Service of Endocrinology, Diabetes and Metabolism, Lausanne University Hospital, Lausanne, Switzerland

<sup>8</sup>Department of Human Genetics and Radboud Institute for Molecular Life Sciences (RIMLS), Radboud University Medical Center, Nijmegen, The Netherlands

<sup>9</sup>Medical Proteome Center, Institute for Ophthalmic Research, University of Tuebingen, Tuebingen, Germany

<sup>10</sup>Department of Ophthalmology, Jules Gonin Ophthalmic Hospital, Lausanne, Switzerland

<sup>11</sup>Donders Center for Neuroscience, Radboud University, Nijmegen, The Netherlands



## Abstract

Cone-rod degeneration (CRD) belongs to the disease spectrum of retinal degenerations, a group of hereditary disorders characterized by an extreme clinical and genetic heterogeneity. It mainly differentiates from other retinal dystrophies, and in particular from the more frequent disease retinitis pigmentosa, because cone photoreceptors degenerate at a higher rate than rod photoreceptors, causing severe deficiency of central vision. Following exome analysis of a cohort of patients with CRD, we identified biallelic mutations in the orphan gene *CEP78* in three patients from two families: one from Greece and another from Sweden. The Greek patient was homozygous for the IVS3+1G>T (c.499+1G>T) mutation in intron 3, likely as a consequence of a mutational founder effect in the island of Crete. The Swedish patients, two siblings, were compound heterozygotes for the nearby mutation IVS3+5G>A (c.499+5G>A) and for the frameshift-causing variant c.633delC; p.Trp212GlyfsTer18. In addition to CRD, all patients had hearing loss or borderline hearing deficit. Immunostaining revealed the presence of CEP78 in the inner segments of retinal photoreceptors, predominantly of cones, and at the base of the primary cilium of fibroblasts. Interaction studies also showed that CEP78 binds to FAM161A, another ciliary protein associated with retinal degeneration. Finally, analysis of skin fibroblasts derived from patients revealed abnormal ciliary morphology, compared to control cells. Altogether, our data strongly suggest that mutations in *CEP78* cause a novel clinical entity of ciliary nature, characterized by blindness and deafness but clearly distinct from Usher syndrome, a condition for which visual impairment is due to retinitis pigmentosa.

Cone-rod degeneration (CRD, MIM 120970) represents an extremely rare class of hereditary diseases that affect the light-sensing neurons of the retina, the cone and rod photoreceptors.<sup>1</sup> Cones are involved in daytime vision, providing the brain with color information and central, precise visual input. Conversely, rods are active in very dim light conditions, are more abundant in retinal periphery, and produce achromatic information, typical for instance of the visual stimulation provided by a landscape in a moonless night. Patients with CRD typically experience initial loss of visual acuity (central vision) and aberrant color vision, due to the prominent loss of cones, while rod functions remain relatively preserved.<sup>2</sup> As the disease progresses, both cone and rod functions deteriorate, central vision is severely impaired or lost, while peripheral islands of the retina may retain some residual activity.<sup>3</sup> Based on these clinical parameters, CRD can be distinguished from retinitis pigmentosa (also called rod-cone degeneration), the most common form of hereditary retinal degeneration. In retinitis pigmentosa rods are more severely affected than cones, initial symptoms include night blindness (nyctalopia), and central vision is often preserved until the very late stages of the disease.<sup>4</sup> CRD is almost invariably inherited as a Mendelian trait, predominantly according to a recessive pattern of transmission, and is characterized by an elevated genetic and allelic heterogeneity.<sup>5</sup> Although as many as 33 CRD-associated genes have been identified to date (<https://sph.uth.edu/Retnet/>), they are found to be mutated in only ~25% of clinical cases, implying that a substantial percentage of patients may carry mutations in genes yet to be identified.<sup>6</sup>

Following this rationale, we performed Whole-Exome Sequencing (WES) in 34 unrelated patients with CRD (29 from Greece and 5 from Sweden). Upon signature of a consent form, genomic DNA was extracted from peripheral blood leukocytes following standard procedures, and then exomic libraries (SureSelect V5 kit, Agilent) were sequenced

on an Illumina HiSeq2000. Raw sequence files were assessed, trimmed, and finally mapped back to the human genome reference sequence (build hg19); DNA variants were called and scored according to a specific *in silico* pipeline, described before.<sup>7</sup> Aggregate data analysis and variant filtering procedures (Table S1) identified biallelic mutations in two index patients, one from Greece and another from Sweden, in *CEP78* (centrosomal protein of 78 kDa gene, composed of 16 exons for its longest coding isoform, NM\_001098802.1). Both patients had classical signs and symptoms of CRD, clearly distinct from retinitis pigmentosa, as detailed below.

The Greek patient (KN10) was a 59 year-old male from the island of Crete, the eldest of two siblings of a non-consanguineous family. His sister was unaffected, and the family reported no history of retinal degeneration (Figure 1). Clinical history indicated hemarelopiia since early adulthood (18-20 years of age) that progressed to severe central vision loss, at the age of 35-40 years, and evolved into severe visual impairment, nystagmus and photophobia. Dyschromatopsia was also reported. Fundus examination showed since the first visit normal color and normal vessels but a small atrophic foveal area with subjacent ring-like glistening in one eye and bull's eye maculopathy in the other eye. A few atrophic lesions were present in the inferior periphery in one eye (Figure 2). The 30 degrees static automated perimetry revealed a diffuse suppression of the visual field in both eyes with a relative conservation of the peripapillary and superior periphery. Full-field electroretinography (ERG) showed flat cone responses but still some residual rod-mediated signals in the left eye. The patient also complained about minor hearing problems and his audiogram exhibited relatively mild deficit; nonetheless, such deficit was clearly distinct and more severe than natural age-related hearing loss (presbycusis)<sup>8</sup> (Figure 2). KN10 carried a homozygous substitution in the first invariant base of intron 3 splice donor site IVS3+1G>T

(c.499+1G>T) (Figure 1). This variant was comprised within a very small stretch of homozygosity that was not statistically significant for autozygosity, possibly indicating a mutational founder effect of geographic origin (not shown). The only relative that could be tested was his paternal uncle, who carried this DNA change heterozygously (Figure 1).

The Swedish index patient (2716s15), now deceased, was last examined at 69 years of age. He was born from unaffected parents and was the first child of a kindred of two. His sister (2702r34), examined at age 65, also had retinal degeneration. Both had visual problems since childhood, including loss of color sensitivity and central vision. Both also reported hearing deficit since younger ages, and both had hearing aids. Audiogram of the living patient at age 66 years revealed substantial sensorineural hearing loss, which did not seem to progress substantially over the following 11 years (Figure 2). Hospital records containing information on the hearing status of her deceased brother were destroyed upon his death. Fundus examination revealed degenerative changes for both siblings in the macular region and some spicular pigment in the mid-periphery but less changes in the periphery (Figure 2). Progressive deterioration of the visual field was reported and documented to expand from the center to the periphery. At last examinations, they both retained some residual vision at the periphery of the visual field, especially in dim light conditions. Similar to the Greek patient, full-field ERG of both individuals highlighted almost no residual cone activity, but revealed still some rod-mediated responses, even at these late ages. These siblings were compound heterozygotes for two *CEP78* mutations: a frameshift-causing single nucleotide deletion (c.633delC; p.Trp212GlyfsTer18) in exon 5 and an intronic base substitution (IVS3+5G>A; c.499+5G>A) in the vicinity of the donor site for intron 3, just 4 nucleotides away from the mutation identified in the Greek patient. Genetic examination

of the index patient's son revealed the presence of this latter mutation in heterozygosis, confirming the biallelic nature of the changes detected in his father and his aunt (Figure 1).

Sanger sequencing of the entire open reading frame of *CEP78* in a cohort of 99 unrelated CRD patients of Swedish, Swiss, Dutch, and Pakistani ethnic background failed to identify any additional causative variants. The three mutations present in our two families were not detected in the genome of an internal control cohort of 350 unrelated individuals or in any other public database, including the 1000 Genomes Project, the Exome Variant Server (EVS, <http://evs.gs.washington.edu/EVS>) and the Exome Aggregation Consortium (ExAC, <http://exac.broadinstitute.org>), which reports sequencing data from more than 61,000 unrelated individuals. In addition, *in silico* assessment of the c.499+1G>T and c.499+5G>A mutations using two distinct web-based platforms, NNSPLICE 0.9<sup>9</sup> and Human Splicing Finder,<sup>10</sup> predicted for both variants the abolishment of the donor splicing site for intron 3.

To analyze the functional consequences of the three identified mutations, we obtained fresh blood samples and skin biopsies from the Greek index patient and the living Swedish patient, and performed the following experiments. We first retrotranscribed total RNA from immortalized lymphoblasts (GoScript™ Reverse Transcriptase, Promega) and then, following saturating RT-PCR of the region spanning all mutations (primers: 5'-TTTTGCAGAAGTCGTGTTTCCT-3' and 5'-TTCAAGGGCCTCTAGCAAAG-3'), we cloned the amplified products in *E. coli* (Zero Blunt® PCR Cloning Kits, Invitrogen) and performed colony PCRs and capillary electrophoresis on 96 clones (48 clones per patient). Representative samples were Sanger sequenced and relative amounts of splicing events were assessed and quantified. The IVS3+1G>T mutation resulted invariantly in the in-frame skipping of exon 3, leading to the production of an aberrant isoform, never reported in genomic databases, for

which exons 2 and 4 were joined together (Figure 1). This event neither altered the open reading frame of *CEP78*, nor led to the formation of a premature termination codon. Therefore, it was predicted not to trigger nonsense-mediated mRNA decay (NMD)<sup>11</sup> but conversely result in the production of a shorter protein, possibly less stable than the wild-type form, lacking the first of five leucine-rich repeat domains (Figure 1). The same exon skipping occurrence was observed for the other, nearby mutation IVS3+5G>A that was present in the Swedish patients. Finally, the frameshift mutation c.633delC resulted in reduced mRNA amounts, as deduced by the low number of *E. coli* colonies carrying this cDNA clone (4 out of 48), again probably due to the action of NMD. Western blot analysis in fibroblasts' extracts (A301-799A-T, Bethyl Laboratories and A2066, Sigma, for beta actin) revealed the presence of a CEP78 protein form having reduced amounts and a comparable molecular weight with respect to controls in the Greek patient, and in no detectable band in the Swedish patient, in agreement with the mRNA findings described above (Figure 3). More specifically, the homozygous IVS3+1G>T mutation likely resulted in proteins lacking the small internal portion corresponding to exon 3 on the DNA sequence and therefore having a minimal difference in molecular weight with respect to the wild-type form. Interestingly, reduced quantities indicated that such mutant protein was indeed less stable than its wild-type counterpart. Concerning the Swedish patient, it is likely that the 633delC allele resulted in no protein at all, as predicted in silico and following mRNA analysis, whereas the IVS3+5G>A allele produced the same form detected in the Greek patient but at non-detectable amounts in standard conditions, due to both putative protein instability and heterozygosity for the mutation. Overexposed films showed in fact a faint band corresponding to CEP78, indicating that the protein was present in trace amounts (not shown).

To gain insights into the relationship between vision and CEP78, we analyzed its expression in a panel of human tissues of cadaveric origin (Human Total RNA Master Panel II, Takara). Despite the levels of *CEP78* transcripts in retina was higher than in many other tissues and organs, retinal *CEP78* mRNA did not display the highest value of expression (Figure 4). A time course experiment on eyes of developing and postnatal mice revealed high expression at embryonic stages, followed by a progressive decrease at perinatal stages, and by a plateau at adulthood (Figure 4). This pattern recalls the expression of other genes involved in retinal degenerations and in early biogenesis and homeostasis of the centriole, notably: *CEP76*, *CEP110*, *CEP164*, *RAB8A*, *BBS4*, and *RPGR*.<sup>12</sup> Although we could not obtain primary data on *CEP78* expression in human cochlea, we assessed its RNAseq values from the only comprehensive transcriptome repository currently available for the inner ear<sup>13</sup> *CEP78* displayed a FPKM (fragments per kilobase of exon per million reads mapped) value of 4.53, as an average obtained from three human cochleae, indicating moderate expression in this structure. Interestingly, the amount of *CEP78* transcripts appeared to be higher than that of most genes already known to be associated with hereditary deafness (40 out of 70, or 57%), assessed in the same organs and in the same conditions (Table S2).

Little is known about the function of CEP78. Identified as a component of the centrosome by two independent proteomic screenings,<sup>14,15</sup> CEP78 is composed of 5 leucine-rich repeats located at the N-terminal half of the protein, as well as a coiled-coil domain at the C-terminus (Figure 1). An important study using *Planaria* as main experimental model revealed that miRNA-based knocking-down of *CEP78* results in defective primary cilia assembly in flatworms and human RPE1 cells.<sup>16</sup> Intriguingly, CEP78 was also found over 5-fold upregulated by noise stress in rat cochlea.<sup>17</sup> The function and impact of CEP78 in human physiology, however, remain largely elusive. Its reported centrosomal localization prompted

us to investigate a possible role for CEP78 in relationship to the connecting cilium of photoreceptors. Immunofluorescence of human retinal sections with anti-CEP78 antibody (IHC-00364-T, Bethyl Laboratories) and anti-cone arrestin (SC-54355, Santa Cruz) revealed that CEP78 is present in dot-shaped foci in the inner segments, likely at the base of the retinal photoreceptors primary cilium, predominantly of cones (Figure 5, Figure S1). This observation was confirmed when CEP78 was labeled together with acetylated tubulin, staining the primary cilium of human skin fibroblasts (Figure 5). Interestingly, positive staining was observed in fibroblasts from KN10 and 2702r34 as well, indicating that *CEP78* was expressed at the protein level in these patients, as predicted (Figure 5). No specific differences concerning CEP78 subcellular localization were observed in cells from patients vs. cells from controls.

Localization at the base of the connecting cilium is a characteristic that is shared by other proteins associated with retinal degeneration, and in particular by FAM161A, the deficiency of which causes the RP28 form of retinitis pigmentosa.<sup>18-20</sup> Tandem-affinity purification analysis performed with full-length FAM161A showed indeed positive interaction with CEP78,<sup>21</sup> and co-immunoprecipitation with an anti-CEP78 antibody (A301-800A, Bethyl Laboratories, epitope between residues 639 and 689) using HEK293T cells transfected with full-length FLAG-FAM161A revealed direct binding between these two ciliary proteins (Figure 5).

Based on these findings, we speculated that CRD due to mutations in *CEP78* could be a consequence of hindered ciliary function, similarly to many other retinal degenerations.<sup>22</sup> To test this hypothesis, we analyzed the morphology of cilia in fibroblasts derived from patients and four controls following serum starvation. Unsupervised counting of at least 82 events per sample (207 events in patients and 430 in controls) revealed that induced cilia in

patient-derived fibroblasts were significantly longer than in controls (Figure 6, Figure S2), a phenomenon that has been previously associated with impaired function of this organelle. For instance, mutations in murine homologues of *BBS4*, *ICK* and *TSC1*, linked with ciliopathies such as Bardet-Biedl syndrome, endocrine-cerebro-osteodysplasia and tuberous sclerosis, respectively, display kidney cells with elongated primary cilia.<sup>23-25</sup>

In recent years a significant, yet expanding number of diverse and degenerative single-gene disorders, have been recognized to fall under the same pathogenesis group featuring aberrant primary cilia function. These diseases, collectively called ciliopathies, form a genetically heterogeneous spectrum of disorders affecting various tissues and organs comprising for instance kidney, cochlea, brain, and retina.<sup>22,26</sup> Classical examples of ciliopathies involving retina and other tissues are Usher syndrome (blindness and deafness) and Bardet-Biedl syndrome (blindness and multi-organ defects) for both of which vision loss is due to recessive retinitis pigmentosa.<sup>27</sup> In addition, syndromic ciliopathies such as Senior-Løken syndrome, Joubert and/or Jeune syndrome may occasionally be accompanied by retinal dystrophy and in particular retinitis pigmentosa and/or Leber Congenital Amaurosis.<sup>28-31</sup> Another multi-organ ciliopathy is Alström syndrome,<sup>32</sup> caused by null mutations in the gene *ALMS1*. This disease is characterized by cone-rod degeneration, dilated cardiomyopathy, obesity, type 2 diabetes, and short stature, which can be accompanied by hepatosteatorosis and defects in lungs, kidney, and bladder.<sup>32,33</sup> Most cases also display progressive sensorineural hearing loss.<sup>34</sup> Of interest, mutations in *ALMS1* have recently been suggested as causative of non-syndromic CRD.<sup>35</sup>

In this study, we show that mutations in *CEP78* result in cone-rod degeneration associated with hearing loss, another hallmark of ciliopathy, but no other syndromic features. Interestingly, the two Swedish patients had declared hearing loss while the Greek

patient had borderline hearing impairment. An intriguing possibility involves the presence of a genotype/phenotype correlation between *CEP78* alleles and hearing (but not vision), as it is the case for instance for mutations in *USH2A* and *ALMS1*.<sup>35-37</sup> Taken together, our data indicate that mutations in *CEP78* define a newly-recognized ciliopathy, distinct from Usher and Alström syndrome, affecting both the visual and the hearing systems.

## Acknowledgements

This work was supported by the Swiss National Science Foundation (grant # 156260, to CR), by the European Community's Seventh Framework Programmes FP7/2009 under grant agreement no: 241955 (SYSCILIA) to R.R. and M.U. and by the Netherlands Organization for Scientific Research (NWO Vici-865.12.005) to R.R., by the Rotterdamse Stichting Blindenbelangen, the Stichting Blindenhulp, the Stichting A.F. Deutman Researchfonds Oogheelkunde, and the Stichting voor Ooglijders (to F.P.M.C. and M.I.K.). F.P.M.C. and M.I.K. were also supported by the following foundations: the Algemene Nederlandse Vereniging ter Voorkoming van Blindheid, the Landelijke Stichting voor Blinden en Slechtienden, the Stichting Retina Nederland Fonds, and the Novartis fund, contributed through Uitzicht. We would also like to acknowledge Drs. Andrea Superti-Furga and Luisa Bonafé from the Center for Molecular Diseases of the Lausanne University Hospital, Dr. Frauke Coppieters from the Ghent University Hospital, Drs. Guy Van Camp from the University of Antwerp, and Dr. Isabelle Schrauwen from the Translational Genomics Research Institute in Phoenix, AZ.

## References

1. Hamel, C.P. (2007). Cone rod dystrophies. *Orphanet J. Rare Dis.* 2, 7.
2. Berson, E.L., Gouras, P., and Gunkel, R.D. (1968). Progressive cone-rod degeneration. *Arch. Ophthalmol.* 80, 68-76.
3. Krauss, H.R., and Heckenlively, J.R. (1982). Visual field changes in cone-rod degenerations. *Arch. Ophthalmol.* 100, 1784-1790.
4. Berson, E.L. (1993). Retinitis pigmentosa. The Friedenwald Lecture. *Invest. Ophthalmol. Vis. Sci.* 34, 1659-1676.
5. Berger, W., Kloeckener-Gruissem, B., and Neidhardt, J. (2010). The molecular basis of human retinal and vitreoretinal diseases. *Prog. Retin. Eye Res.* 29, 335-375.
6. Roosing, S., Thiadens, A.A., Hoyng, C.B., Klaver, C.C., den Hollander, A.I., and Cremers, F.P. (2014). Causes and consequences of inherited cone disorders. *Prog. Retin. Eye Res.* 42, 1-26.
7. Royer-Bertrand, B., Castillo-Taucher, S., Moreno-Salinas, R., Cho, T.J., Chae, J.H., Choi, M., Kim, O.H., Dikoglu, E., Campos-Xavier, B., Girardi, E., et al. (2015). Mutations in the heat-shock protein A9 (HSPA9) gene cause the EVEN-PLUS syndrome of congenital malformations and skeletal dysplasia. *Sci. Rep.* 5, 17154.
8. Jerger, J., Chmiel, R., Stach, B., and Spretnjak, M. (1993). Gender affects audiometric shape in presbycusis. *J. Am. Acad. Audiol.* 4, 42-49.
9. Reese, M.G., Eeckman, F.H., Kulp, D., and Haussler, D. (1997). Improved splice site detection in Genie. *J. Comput. Biol.* 4, 311-323.
10. Desmet, F.O., Hamroun, D., Lalande, M., Collod-Beroud, G., Claustres, M., and Beroud, C. (2009). Human Splicing Finder: an online bioinformatics tool to predict splicing signals. *Nucleic Acids Res.* 37, e67.
11. Hentze, M.W., and Kulozik, A.E. (1999). A perfect message: RNA surveillance and nonsense-mediated decay. *Cell* 96, 307-310.
12. Zhang, S.S., Xu, X., Liu, M.G., Zhao, H., Soares, M.B., Barnstable, C.J., and Fu, X.Y. (2006). A biphasic pattern of gene expression during mouse retina development. *BMC Dev. Biol.* 6, 48.
13. Schrauwen, I., Hasin-Brumshtein, Y., Corneveaux, J.J., Ohmen, J., White, C., Allen, A.N., Lusi, A.J., Van Camp, G., Huentelman, M.J., and Friedman, R.A. (2016). A comprehensive catalogue of the coding and non-coding transcripts of the human inner ear. *Hear. Res.* 333, 266-274.

14. Andersen, J.S., Wilkinson, C.J., Mayor, T., Mortensen, P., Nigg, E.A., and Mann, M. (2003). Proteomic characterization of the human centrosome by protein correlation profiling. *Nature* 426, 570-574.
15. Jakobsen, L., Vanselow, K., Skogs, M., Toyoda, Y., Lundberg, E., Poser, I., Falkenby, L.G., Bennetzen, M., Westendorf, J., Nigg, E.A., et al. (2011). Novel asymmetrically localizing components of human centrosomes identified by complementary proteomics methods. *EMBO J.* 30, 1520-1535.
16. Azimzadeh, J., Wong, M.L., Downhour, D.M., Sanchez Alvarado, A., and Marshall, W.F. (2012). Centrosome loss in the evolution of planarians. *Science* 335, 461-463.
17. Han, Y., Hong, L., Zhong, C., Chen, Y., Wang, Y., Mao, X., Zhao, D., and Qiu, J. (2012). Identification of new altered genes in rat cochleae with noise-induced hearing loss. *Gene* 499, 318-322.
18. Bandah-Rozenfeld, D., Mizrahi-Meissonnier, L., Farhy, C., Obolensky, A., Chowers, I., Pe'er, J., Merin, S., Ben-Yosef, T., Ashery-Padan, R., Banin, E., et al. (2010). Homozygosity mapping reveals null mutations in FAM161A as a cause of autosomal-recessive retinitis pigmentosa. *Am. J. Hum. Genet.* 87, 382-391.
19. Langmann, T., Di Gioia, S.A., Rau, I., Stohr, H., Maksimovic, N.S., Corbo, J.C., Renner, A.B., Zrenner, E., Kumaramanickavel, G., Karlstetter, M., et al. (2010). Nonsense Mutations in FAM161A Cause RP28-Associated Recessive Retinitis Pigmentosa. *Am. J. Hum. Genet.* 87, 376-381.
20. Di Gioia, S.A., Letteboer, S.J., Kostic, C., Bandah-Rozenfeld, D., Hettterschijt, L., Sharon, D., Arsenijevic, Y., Roepman, R., and Rivolta, C. (2012). FAM161A, associated with retinitis pigmentosa, is a component of the cilia-basal body complex and interacts with proteins involved in ciliopathies. *Hum. Mol. Genet.* 21, 5174-5184.
21. Di Gioia, S.A. (2013). Targeted sequence capture and ultra high throughput sequencing for gene discovery in inherited diseases. PhD Thesis, University of Lausanne, Lausanne, Switzerland.
22. Wright, A.F., Chakarova, C.F., Abd El-Aziz, M.M., and Bhattacharya, S.S. (2010). Photoreceptor degeneration: genetic and mechanistic dissection of a complex trait. *Nat. Rev. Genet.* 11, 273-284.
23. Armour, E.A., Carson, R.P., and Ess, K.C. (2012). Cystogenesis and elongated primary cilia in Tsc1-deficient distal convoluted tubules. *Am. J. Physiol. Renal Physiol.* 303, F584-592.
24. Moon, H., Song, J., Shin, J.O., Lee, H., Kim, H.K., Eggenschwiller, J.T., Bok, J., and Ko, H.W. (2014). Intestinal cell kinase, a protein associated with endocrine-cerebro-osteodysplasia syndrome, is a key regulator of cilia length and Hedgehog signaling. *Proc. Natl. Acad. Sci. U. S. A.* 111, 8541-8546.

25. Mokrzan, E.M., Lewis, J.S., and Mykytyn, K. (2007). Differences in renal tubule primary cilia length in a mouse model of Bardet-Biedl syndrome. *Nephron Exp Nephrol* *106*, e88-96.
26. Waters, A.M., and Beales, P.L. (2011). Ciliopathies: an expanding disease spectrum. *Pediatr. Nephrol.* *26*, 1039-1056.
27. Koenig, R. (2003). Bardet-Biedl syndrome and Usher syndrome. *Dev. Ophthalmol.* *37*, 126-140.
28. Bachmann-Gagescu, R., Dempsey, J.C., Phelps, I.G., O'Roak, B.J., Knutzen, D.M., Rue, T.C., Ishak, G.E., Isabella, C.R., Gordon, N., Adkins, J., et al. (2015). Joubert syndrome: a model for untangling recessive disorders with extreme genetic heterogeneity. *J. Med. Genet.* *52*, 514-522.
29. Bard, L.A., Bard, P.A., Owens, G.W., and Hall, B.D. (1978). Retinal involvement in thoracic-pelvic-phalangeal dystrophy. *Arch. Ophthalmol.* *96*, 278-281.
30. Wilson, D.J., Weleber, R.G., and Beales, R.K. (1987). Retinal dystrophy in Jeune's syndrome. *Arch. Ophthalmol.* *105*, 651-657.
31. Hildebrandt, F., and Zhou, W. (2007). Nephronophthisis-associated ciliopathies. *J. Am. Soc. Nephrol.* *18*, 1855-1871.
32. Marshall, J.D., Muller, J., Collin, G.B., Milan, G., Kingsmore, S.F., Dinwiddie, D., Farrow, E.G., Miller, N.A., Favaretto, F., Maffei, P., et al. (2015). Alstrom Syndrome: Mutation Spectrum of ALMS1. *Hum. Mutat.* *36*, 660-668.
33. Marshall, J.D., Maffei, P., Collin, G.B., and Naggert, J.K. (2011). Alstrom syndrome: genetics and clinical overview. *Curr. Genomics* *12*, 225-235.
34. Marshall, J.D., Bronson, R.T., Collin, G.B., Nordstrom, A.D., Maffei, P., Paisey, R.B., Carey, C., Macdermott, S., Russell-Eggitt, I., Shea, S.E., et al. (2005). New Alstrom syndrome phenotypes based on the evaluation of 182 cases. *Arch. Intern. Med.* *165*, 675-683.
35. Lazar, C.H., Kimchi, A., Namburi, P., Mutsuddi, M., Zelinger, L., Beryozkin, A., Ben-Simhon, S., Obolensky, A., Ben-Neriah, Z., Argov, Z., et al. (2015). Nonsyndromic Early-Onset Cone-Rod Dystrophy and Limb-Girdle Muscular Dystrophy in a Consanguineous Israeli Family are Caused by Two Independent yet Linked Mutations in ALMS1 and DYSF. *Hum. Mutat.* *36*, 836-841.
36. Rivolta, C., Sweklo, E.A., Berson, E.L., and Dryja, T.P. (2000). Missense mutation in the USH2A gene: association with recessive retinitis pigmentosa without hearing loss. *Am. J. Hum. Genet.* *66*, 1975-1978.
37. Lenassi, E., Vincent, A., Li, Z., Saihan, Z., Coffey, A.J., Steele-Stallard, H.B., Moore, A.T., Steel, K.P., Luxon, L.M., Heon, E., et al. (2015). A detailed clinical and molecular survey of subjects with nonsyndromic USH2A retinopathy reveals an allelic hierarchy of disease-causing variants. *Eur. J. Hum. Genet.* *23*, 1318-1327.

38. Cruickshanks, K.J., Wiley, T.L., Tweed, T.S., Klein, B.E., Klein, R., Mares-Perlman, J.A., and Nondahl, D.M. (1998). Prevalence of hearing loss in older adults in Beaver Dam, Wisconsin. The Epidemiology of Hearing Loss Study. *Am. J. Epidemiol.* *148*, 879-886.

## Legends to Figures

**Figure 1. *CEP78* mutations.** (A) Pedigrees and electropherograms of the DNA changes identified. Asterisks indicate the site of mutations. Mx, mutant alleles; wt, wild-type allele. (B) Schematic structure of the *CEP78* gene and protein and effects of mutations. (B) The longest *CEP78* coding isoform is composed of 16 exons (white boxes), resulting in a 78 kDa protein (grey bar) bearing 5 leucine-rich repeat domains (LRRx, red boxes) and one coiled coil domain (CC, green box). Mutations M1 and M2 lead to transcripts lacking exon 3 and, since there is no shift of the reading frame, likely to a CEP78 protein form lacking the first leucine-rich repeat domain. Conversely, M3 alleles result in aberrant transcripts bearing a shift of the reading frame (fs, blue box) that are susceptible to be inactivated by nonsense-mRNA decay (NMD).

**Figure 2. Clinical features of patients.** (A) Patient KN10. Fundus pictures (at age 53 years) reveal macular coalescent hypochromatic lesions in the right eye and minor macular changes in the left eye. Pure tone audiograms at age 57 years (black lines) and 59 years (red lines) show mild hearing impairment at higher frequencies compared to the normal range for gender and age, indicated by the shaded area.<sup>38</sup> (B) Patient 2702r34. Fundus examination at age 65 years highlights attenuated vessels and degenerative changes in the posterior pole. Audiograms at age 66 years (black lines) and 77 years (red lines) show clear hearing loss at most frequencies. OD, right eye; OS, left eye; RE, right ear; LE, left ear.

**Figure 3. Western blot analysis of endogenous CEP78 in fibroblasts from patients.** Numbers on the left refer to molecular size markers. Control, human fibroblasts from a

control individual; HEK293T, Human Embryonic Kidney 293 cells, containing SV40 Large T-antigen, as a control for specificity of the anti-CEP78 antibody.

**Figure 4. CEP78 mRNA expression in various human tissues and organs and in the developing murine eye.** Data are from Real-Time PCR relative expression analysis by using *GUSB* and *HPRT1* as normalizing genes for panel A and B, respectively.

**Figure 5. CEP78 in human cells and its interaction with FAM161A.** (A) Immunostaining of CEP78 (red dots) and of cone arrestin (green) in a section of human retina. Margins of a cone photoreceptor are highlighted by a dotted line. Scale bar: 10  $\mu\text{m}$ . (B). Co-immunoprecipitation of endogenous CEP78 and FLAG-tagged FAM161A, in HEK293T cells. FLAG-SOX4 is a negative control. IP:x, protein targeted by the antibody used in immunoprecipitation; WB:x, protein or peptide targeted by the antibody used in western blots. (C) Staining of CEP78 (red) and acetylated tubulin (green) in fibroblasts from a control individual and patients KN10 and 2702r34. CEP78 localizes at the centrioles and at the base of the induced primary cilium. Scale bars: 5  $\mu\text{m}$  and 1  $\mu\text{m}$  for regular and magnification panels, respectively.

**Figure 6. Analysis of ciliary lengths.** Fibroblasts from patients display significantly longer primary cilia than those from four unaffected controls, suggesting impaired functionality.

Patient	KN10	2716s15
Number of exonic and splicing variants	22,956	22,299
Number of non-synonymous variants	11,347	11,012
Number of rare variants (<1%)	663	527
Number of rare variants after quality control (QC)	335	212
Number of genes with homozygous variants	7	3
Number of genes with 2 heterozygous variants	15	6
Genes in common	<i>CEP78</i> and <i>TTN</i>	

**Table S1. Overview of exonic and splicing variants observed in the two patients, following sequential filtering procedures.** Values refer to number of variants unless specified otherwise. Rare (<1%): Variant frequency = 1% or less in public databases – ExAC, ESP, and Welllderly, 1KG (from Complete Genomics). QC: Rare variants after quality control, i.e. after removal of (1) WES data of poor quality, with less than 15 reads per nucleotide and genotype quality less than 50, (2) variants present in control WES processed by the same pipeline (to remove any technical errors), and (3) variants carried by healthy homozygous individuals in public database (e.g. ExAC). The gene *TTN* appears frequently as a false positive finding in WES studies.

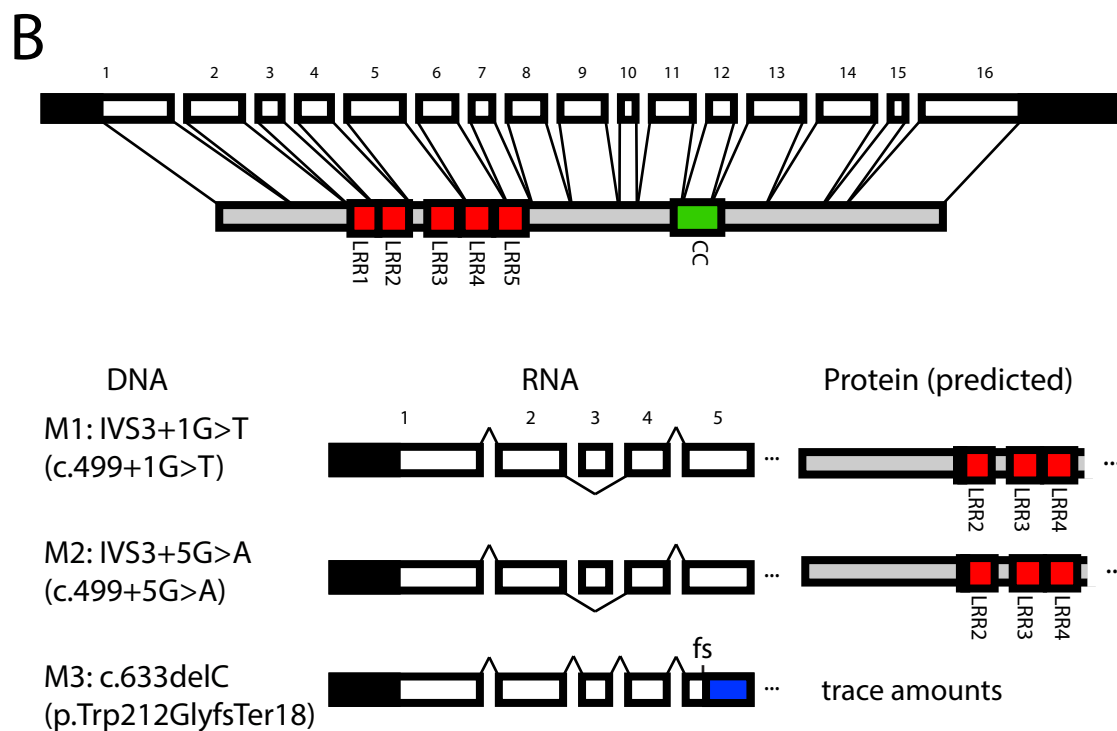
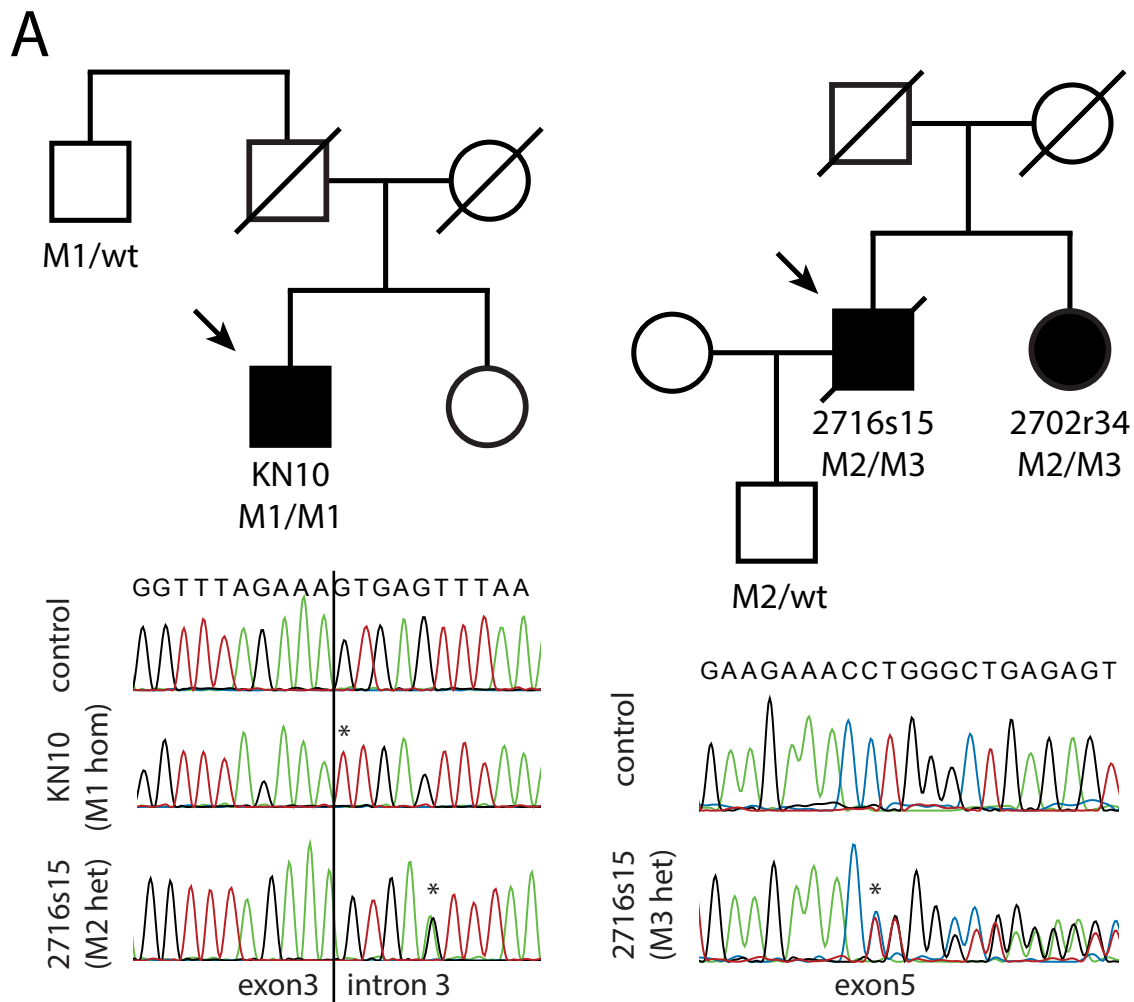


Figure 1

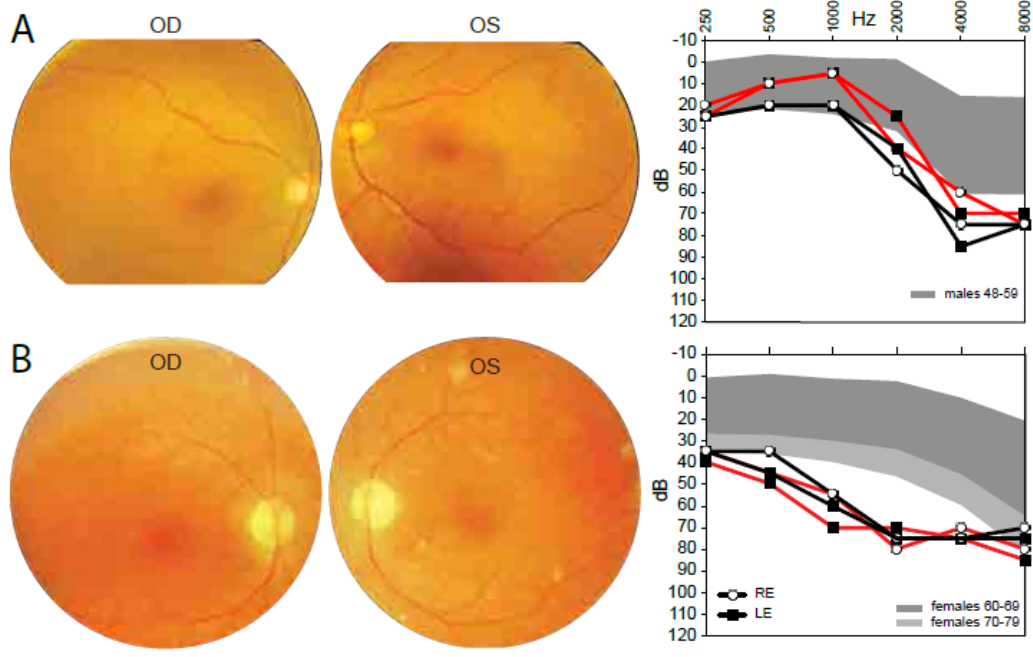


Figure 2

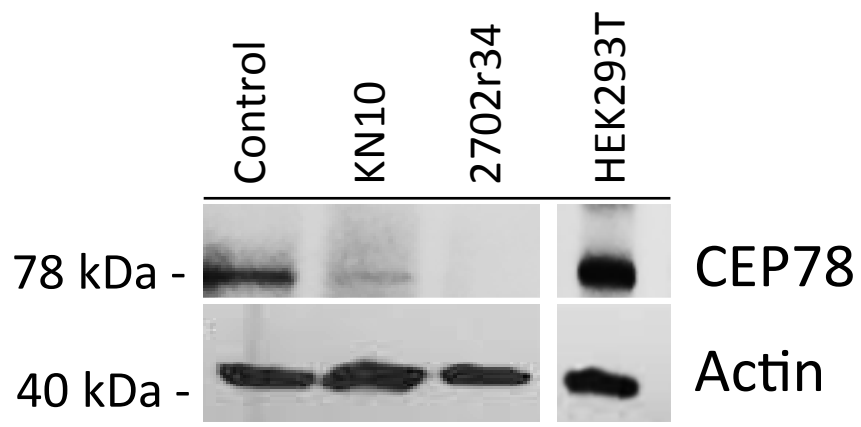


Figure 3

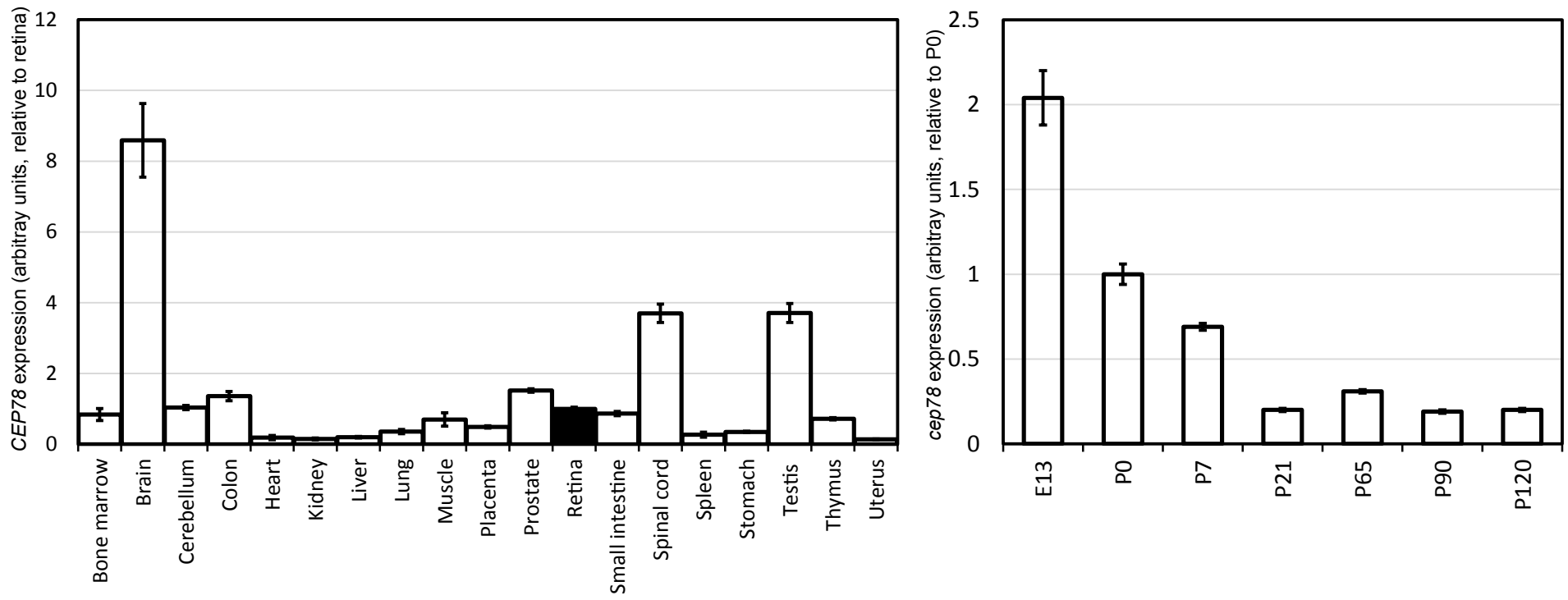


Figure 4

gene_id	gene_name	Coch 1	Coch 2	Coch 3	Average
ENSG00000100000	POU4F3	0	0	0	0
ENSG00000100000	MYO3A	0.000635	0.004849	0.022596	0.00936
ENSG00000100000	SLC17A8	0.000389	0.000547	0.032021	0.010986
ENSG00000100000	LOXHD1	0.025365	0.060565	0.0066	0.030843
ENSG00000100000	GIPC3	0.024089	0.076229	0.039106	0.046475
ENSG00000100000	TMIE	0	0.06341	0.146477	0.069962
ENSG00000100000	PTPRQ	0.006097	0.112682	0.099155	0.072645
ENSG00000100000	CABP2	0.040399	0.173213	0.056216	0.089943
ENSG00000100000	OTOF	0.057953	0.003852	0.223894	0.095233
ENSG00000100000	STRC	0.12565	0.132264	0.119115	0.125676
ENSG00000100000	SLC26A5	0.129152	0.092504	0.255584	0.15908
ENSG00000100000	TPRN	0.094411	0.104095	0.326162	0.174889
ENSG00000100000	METTL12	0.564632	0.064836	4.28E-32	0.209823
ENSG00000100000	P2RX2	0.154111	0.470321	0.119013	0.247815
ENSG00000100000	OTOA	0.00562	0.127403	0.668946	0.267323
ENSG00000100000	TMC1	0.264026	0.366298	0.209721	0.280015
ENSG00000100000	ILDR1	0.221374	0.105951	0.538851	0.288725
ENSG00000100000	GRXCR1	0.012123	0.461481	0.436519	0.303374
ENSG00000100000	BSND	0.152115	0.492989	0.344713	0.329939
ENSG00000100000	KCNQ4	0.095	0.904738	0.154929	0.384889
ENSG00000100000	ESPN	0.194628	0.853735	0.111057	0.386473
ENSG00000100000	MYO7A	0.52261	0.257552	0.428576	0.402913
ENSG00000100000	DCDC2	1.67294	0.284403	0.334591	0.763978
ENSG00000100000	PCDH15	0.253788	1.64893	0.788694	0.897137
ENSG00000100000	CEACAM16	0.013226	0.570029	2.18102	0.921425
ENSG00000100000	METTL15	1.24601	0.662215	1.06318	0.990468
ENSG00000100000	GPSM2	0.283602	1.17825	1.86853	1.110127
ENSG00000100000	MYO15A	1.31241	1.0893	1.4237	1.275137
ENSG00000100000	CLDN14	0.123397	0.915213	2.79064	1.276417
ENSG00000100000	SLC26A4	1.17451	1.33071	1.34425	1.283157
ENSG00000100000	TECTA	2.24775	1.5015	0.631862	1.460371
ENSG00000100000	CIB2	2.28468	0.808458	1.45781	1.516983
ENSG00000100000	METTL4	1.32381	1.23014	2.15561	1.569853
ENSG00000100000	TMPRSS3	2.1716	1.13005	2.42714	1.909597
ENSG00000100000	MARVELD2	1.52109	2.19185	2.07644	1.929793
ENSG00000100000	PTPRN2	1.97559	1.41402	2.79015	2.05992
ENSG00000100000	CDH23	2.65421	2.50604	1.47115	2.210467
ENSG00000100000	HGF	1.20093	4.00613	1.92118	2.37608
ENSG00000100000	ESRRB	1.27515	3.85601	3.7147	2.94862
ENSG00000100000	OSBPL2	4.65872	4.52819	4.36676	4.51789
ENSG00000100000	CEP78	4.50804	2.30044	6.7815	4.529993
ENSG00000100000	METTL3	4.32555	5.5211	4.21988	4.688843
ENSG00000100000	METTL17	6.26857	3.73464	5.09427	5.032493
ENSG00000100000	DFNA5	2.09614	3.53489	9.83763	5.15622
ENSG00000100000	MYH14	5.2459	5.24015	5.54507	5.343707
ENSG00000100000	DIAPH1	6.75299	6.37873	5.71255	6.281423
ENSG00000100000	MSRB3	8.75399	4.9088	7.14766	6.936817
ENSG00000100000	PRDX2	7.68825	5.19914	8.5183	7.13523
ENSG00000100000	CCDC50	5.48502	8.655	8.96887	7.702963

ENSG0000(FAM65B)	9.52451	5.83092	7.94286	7.766097
ENSG0000(WFS1)	13.7706	3.90427	6.26541	7.980093
ENSG0000(PRPS1)	6.76141	9.64509	7.9225	8.109667
ENSG0000(TRIOBP)	8.23531	9.62484	8.07235	8.644167
ENSG0000(TJP2)	10.16	11.5985	5.61086	9.12312
ENSG0000(SERPINB6)	9.76828	9.82138	8.69881	9.42949
ENSG0000(POU3F4)	14.6888	15.8231	20.3449	16.95227
ENSG0000(MET)	19.6721	23.953	8.66128	17.42879
ENSG0000(KARS)	22.3542	20.2033	24.4067	22.3214
ENSG0000(SIX1)	31.1925	21.4469	17.086	23.2418
ENSG0000(MYH9)	30.2774	26.0357	16.2673	24.19347
ENSG0000(EYA4)	30.046	16.2611	31.7525	26.01987
ENSG0000(SMPX)	15.8038	10.495	55.7151	27.33797
ENSG0000(MYO6)	28.8111	32.6395	35.8846	32.44507
ENSG0000(USH1C)	30.8977	21.6356	50.2302	34.2545
ENSG0000(RDX)	57.7042	35.1006	32.5633	41.78937
ENSG0000(EPS8)	49.8291	34.1867	44.4353	42.81703
ENSG0000(GJB6)	157.935	24.7138	78.0029	86.8839
ENSG0000(COL11A2)	133.261	88.6713	257.319	159.7504
ENSG0000(GJB2)	384.907	81.9362	257.936	241.5931
ENSG0000(ACTG1)	808.74	427.013	462.764	566.1723
ENSG0000(COCH)	3679.96	819.586	4595.38	3031.642

Data from: <https://www.tgen.org/home/research/research-divisions/neurogenomics/supplementary-data/inner-ear-transcriptome.aspx#.VzHZXuQkqqw>

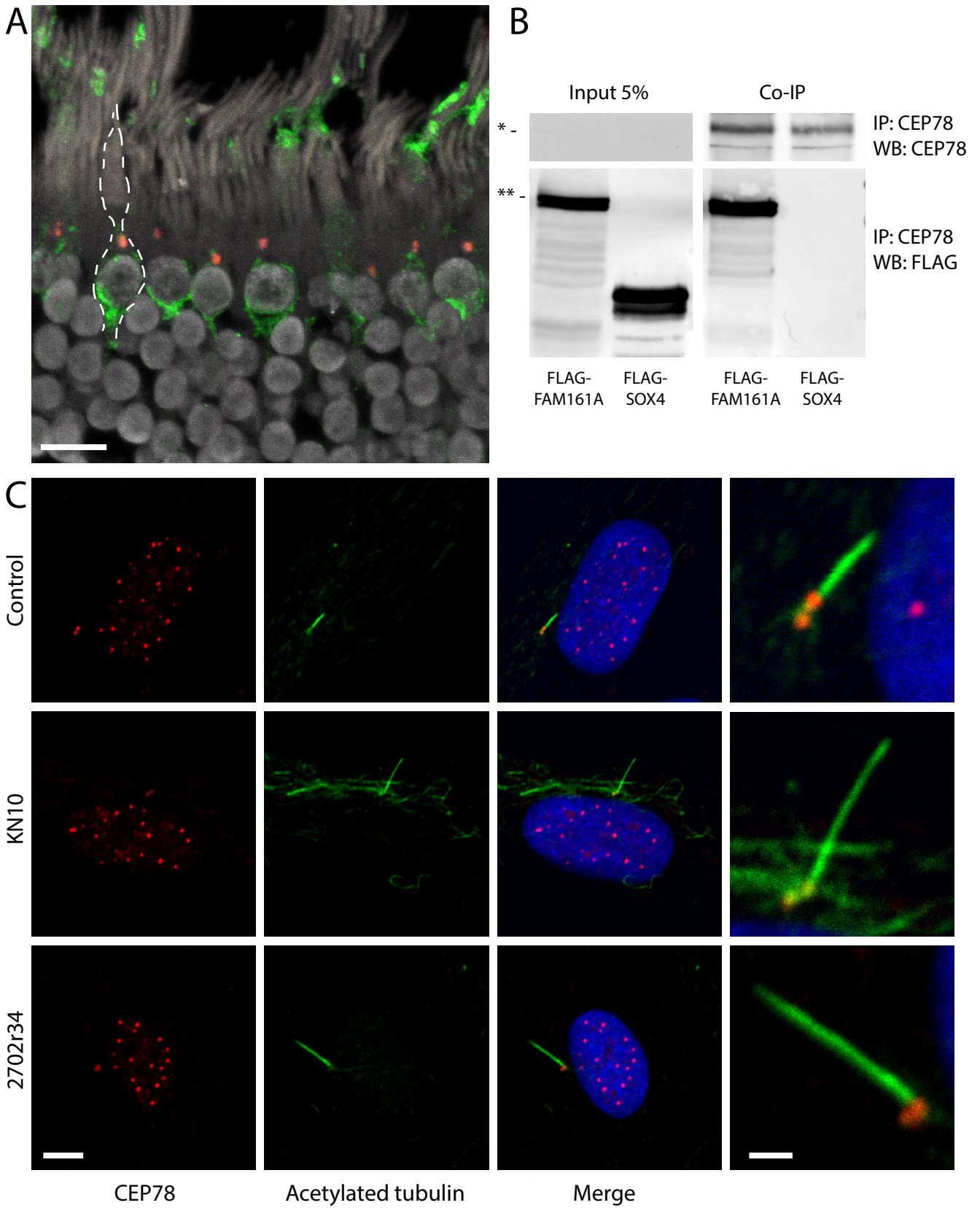
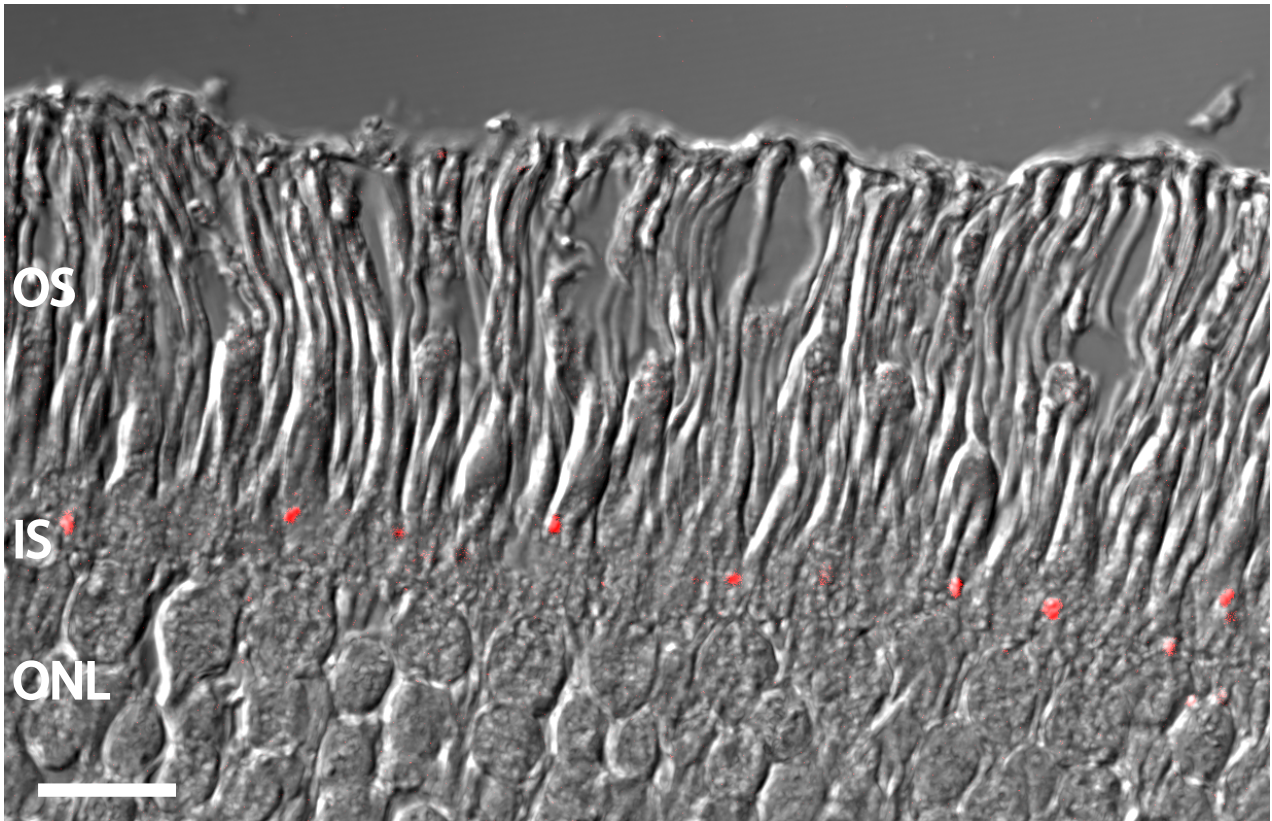


Figure 5



**Figure S1.** Immunostaining of CEP78 in a section of human retina (red dots) reveals its presence in the inner segment (IS) of photoreceptors, likely at the base of the connecting cilium. OS, outer segments; ONL, outer nuclear layer. Scale bar: 10  $\mu\text{m}$ .

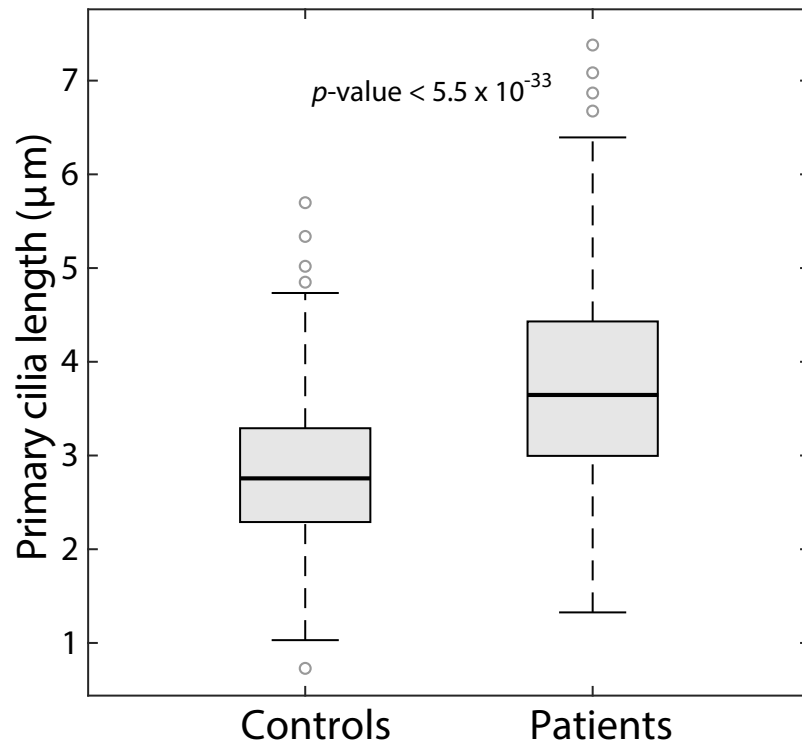
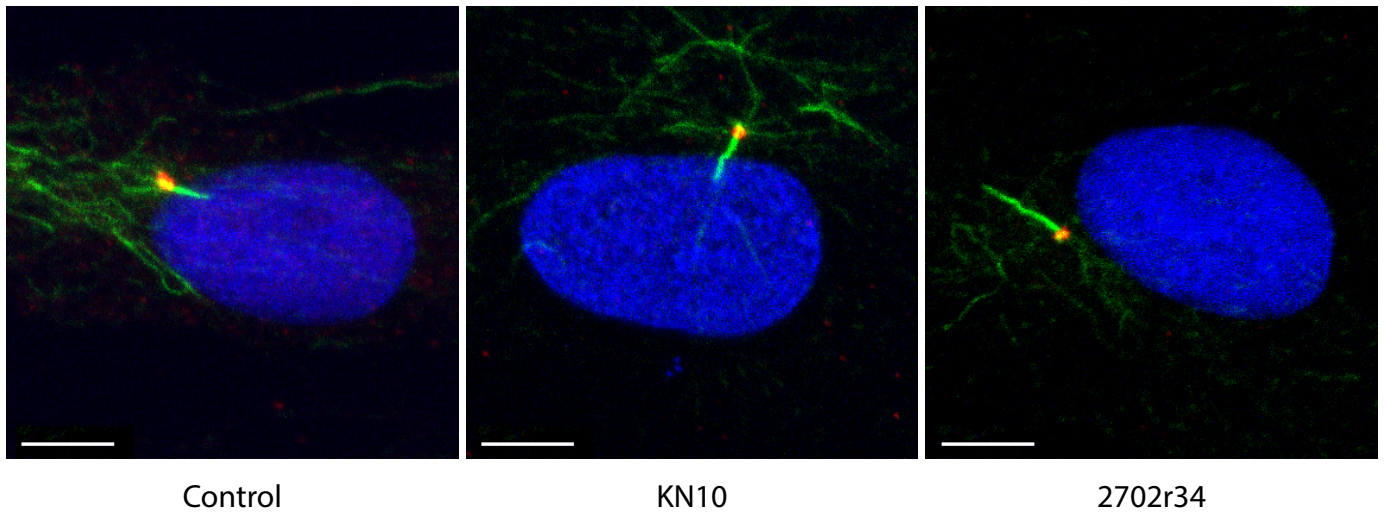


Figure 6



**Figure S2:** Representative samples of the images used for the analysis of cilia lengths, displayed in Figure 6. Green, acetylated tubulin, marking the ciliary axoneme; red, ninein, marking the base of the cilium. Scale bar: 5  $\mu\text{m}$ .